



A novel route to Pt–Bi₂O₃ composite thin films and their application in photo-reduction of water

Savio J.A. Moniz^a, Davinder Bhachu^a, Chris S. Blackman^{a,b,*}, Alison J. Cross^a, Sofia Elouali^a, David Pugh^a, Raul Quesada Cabrera^a, Stella Vallejos^a

^a Materials Chemistry Centre, Department of Chemistry, University College London, 20 Gordon Street, London WC1H 0AJ, UK

^b London Centre for Nanotechnology, 17–19 Gordon Street, London WC1H 0AH, UK

ARTICLE INFO

Article history:

Available online 22 September 2011

Young Investigator Award Special Issue

Keywords:

Bismuth oxide

CVD

Composite

Water reduction

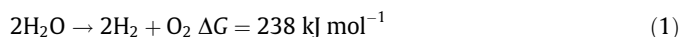
ABSTRACT

A novel homoleptic bismuth(III) β-diketonate (dibenzoylmethane – dbm) complex [Bi(dbm)₃]₂ has been used as a precursor to thin films of crystalline β-Bi₂O₃, and hexachloroplatinic acid (H₂PtCl₆·6H₂O) has been demonstrated as a suitable precursor for deposition of platinum nanoparticles, both deposited via aerosol-assisted chemical vapour deposition (AACVD). Thin films of Pt–Bi₂O₃ were co-deposited from a mixture of [Bi(dbm)₃]₂ and H₂PtCl₆·6H₂O; the introduction of Pt particles into β-Bi₂O₃ causes hydrogen to be evolved during photolysis of water over the composite material, a property not found for Pt particles or β-Bi₂O₃ alone.

© 2011 Elsevier B.V. All rights reserved.

1. Introduction

The ever increasing cost, limited availability and environmental impact of the use of fossil fuels has provided impetus to the search for alternative energy sources that can provide cheap, clean fuel. The use of hydrogen as a renewable chemical fuel source would go some way to decrease greenhouse gas emissions and lessen our dependence on non-renewables [1]. At present, the majority of hydrogen is produced via steam reforming of natural gas, emitting CO₂ in the process. An alternative method of hydrogen production is via water splitting, a process which is accompanied by a large increase in free energy as shown in Eq. (1):



To promote this reaction energy must be input into the system. One of the methods with greatest potential is *via* solar irradiation of a semiconductor, in which the absorbed photons provide the required energy with photo-generated electrons responsible for the reduction of water to H₂ and photo-generated holes for the oxidation to O₂. The most common materials used for water photolysis are metal oxides because they can be made by low cost routes and are more stable in aqueous environments than non-oxide semiconductors. However many transition metal oxides have band gaps which are too large to serve as efficient water-splitting

photo-catalysts under solar irradiation, typically of the order 3.0 eV (Fig. 1), with only ~5% of the solar spectrum having sufficient energy to produce photo-excited electron/hole pairs.

Bismuth(III) oxide, in which the conduction band is principally Bi 6p in character [2], possesses band gap values of 2.29–3.31 eV depending on the phase present [3], potentially extending the region of the solar spectrum that can be utilised for photo-chemistry into the visible region where more energy is available. Indeed we have recently demonstrated that thin films of β-Bi₂O₃ are able to photo-oxidise water with high efficiency [4]. For photo-reduction of water however the conduction band potential of bismuth oxide is not sufficient to be able to evolve hydrogen under photo-irradiation (Fig. 1). Various methods exist for modifying the photo-catalytic properties of a semiconductor, for instance the addition of metal particles can act to ‘trap’ electrons photo-excited in the semiconductor, reducing the overall probability of electron–hole recombination and so increasing the overall efficiency of the photo-system [5]. If made sufficiently reducing by accumulated negative charge these metal particles will readily reduce water to H₂ [6]. Therefore one method for obtaining the potential benefit of the relatively narrow band gap of bismuth(III) oxide for solar hydrogen generation would be to combine it with co-catalyst platinum particles.

We have recently demonstrated the co-deposition of metal nanoparticles and a metal oxide using a simple aerosol-assisted chemical vapour deposition (AACVD) method [7]. The use of AACVD has many potential advantages over other methods of producing composite materials, for instance combining materials synthesis and device fabrication in a single step, and it is also a

* Corresponding author at: Materials Chemistry Centre, Department of Chemistry, University College London, 20 Gordon Street, London WC1H 0AJ, UK. Tel.: +44 0 2076794703.

E-mail address: c.blackman@ucl.ac.uk (Chris S. Blackman).

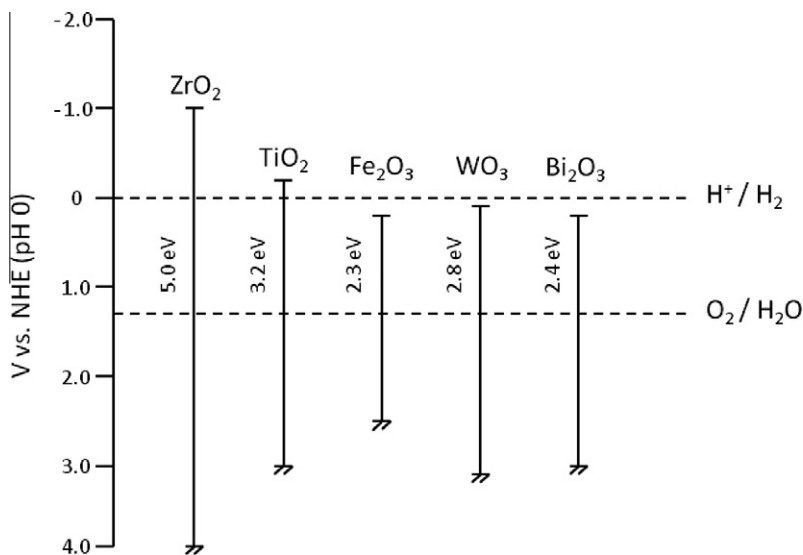


Fig. 1. Band structures of some common binary metal oxides and their relationship to the redox potentials of water splitting at pH 0.

relatively low cost technique, with the ability to cover large surface areas with relatively short deposition times. The use of a liquid aerosol to transport reactants in AACVD allows the use of precursors that are not sufficiently volatile or thermally stable for transport in atmospheric or low pressure CVD experiments to be utilised, for instance relatively inexpensive but thermally unstable HAuCl_4 was used as the gold precursor in the AACVD co-deposition of tungsten oxide with Au-nanoparticles [7]. Surprisingly, despite the use of HAuCl_4 as a precursor to gold nanoparticles *via* AACVD no equivalent chemistry of H_2PtCl_6 has been reported, despite it possessing favourable thermal decomposition characteristics [8].

Unfortunately for the co-deposition of Pt– Bi_2O_3 thin films *via* AACVD H_2PtCl_6 attacks many of the common precursors to bismuth oxide. For instance the donor-functionalised monomeric alkoxide complex $[\text{Bi}(\text{mmp})_3]$ (mmp = 1-methoxy-2-methyl-2-propanolato) [9] and bismuth *tert*-butoxide $[\text{Bi}(\text{O}^t\text{Bu})_3]$ [4] both decomposed in the presence of H_2PtCl_6 . Triphenylbismuth is by far the most commonly used bismuth CVD precursor owing to its high air and moisture stability [10,11], however this low reactivity requires the use of a highly reactive oxygen source which is not compatible with the AACVD method. Bismuth tetramethylheptanedionate, $[\text{Bi}(\text{thd})_3]_2$, has previously been used to deposit bismuth oxide films [12] however it decomposed instantly in solutions containing H_2PtCl_6 . The novel homoleptic β -diketonate complex $[\text{Bi}(\text{dbm})_3]_2$ has been synthesised and structurally characterised, with the complex showing appreciable air and moisture stability and acceptable, although finite, stability in the presence of $\text{H}_2\text{PtCl}_6 \cdot 6\text{H}_2\text{O}$. We report the AACVD deposition of thin films of platinum nanoparticles from $\text{H}_2\text{PtCl}_6 \cdot 6\text{H}_2\text{O}$, Bi_2O_3 films from $[\text{Bi}(\text{dbm})_3]_2$ and platinum nanoparticle-modified Bi_2O_3 films from a mixture of $[\text{Bi}(\text{dbm})_3]_2$ and $\text{H}_2\text{PtCl}_6 \cdot 6\text{H}_2\text{O}$. These have been fully characterised and Pt– Bi_2O_3 thin films demonstrated to reduce water to hydrogen under simulated solar irradiation.

2. Experimental procedures

2.1. General procedures

All reactions were performed under a dry, oxygen-free nitrogen atmosphere using standard Schlenk techniques and an MBraun Unilab glove box. Nitrogen (99.996%) was obtained from BOC and used as supplied. Solvents were dried over alumina columns

(Anhydrous Engineering) and stored over sodium. All reagents were used without further purification, and were procured from Sigma–Aldrich or Alfa Aesar Ltd.

2.2. Physical measurements

Microanalytical data were obtained at University College London (UCL). NMR spectra were recorded on Bruker AMX 500 machines referenced to C_6D_6 distilled over sodium/benzophenone. ^1H and $^{13}\text{C}\{^1\text{H}\}$ chemical shifts are reported relative to SiMe_4 ($\delta = 0.00$ ppm). FT-IR spectra were recorded on a Perkin Elmer Spectrum RX I instrument, over the range $4000\text{--}400\text{ cm}^{-1}$. Mass spectra were recorded on a Micromass ZABSE instrument. Coupled Thermogravimetric Analysis Mass Spectrometry (TGA-MS) was performed on a Netzsch STA 449C instrument using sealed aluminium pans, pierced with a hole at the top prior to heating at atmospheric pressure, under a flow of helium gas (50 sccm); the rate of heating was $10\text{ }^\circ\text{C min}^{-1}$. For single crystal X-ray diffraction crystals were mounted under nitrogen on a glass fibre from Fomblin vacuum oil. Geometric and intensity data were obtained on a Bruker SMART APEX CCD diffractometer using graphite-monochromated Mo $\text{K}\alpha$ radiation ($\lambda_1 = 0.71073\text{ \AA}$) at $150(2)\text{ K}$. Data reduction and integration was carried out with SAINT+ and absorption corrections applied using SADABS [13]. The solution and refinements were performed using PLATON [14], the WINGX package and all software packages within [15]. Hydrogen atoms were placed in geometrically assigned positions with fixed bond lengths of 0.95 \AA . These were refined using a riding model with a $U_{\text{iso}}(\text{H})$ value of $1.2 U_{\text{eq}}$ of the parent atom. Wavelength dispersive X-ray spectroscopy (WDX) of the films was performed on a Philips XL30ESEM machine. Scanning electron microscope (SEM) images were obtained on a JSM-6301F Scanning Microscope Field Emission machine after coating samples with an ultrathin layer of gold (not observed in images) to avoid charging. Grazing incidence (5°) powder X-ray diffraction (XRD) was carried out on a Bruker AXS D8 Discover machine using monochromatic Cu $\text{K}\alpha$ radiation ($\lambda_1 = 1.54056\text{ \AA}$) and a GADDS Area Detector with phase information obtained via the EVA suite of programs (version 2). UV–Vis spectra were recorded in transmission mode over the range $175\text{--}2500\text{ nm}$ using a Perkin Elmer Lambda 950 photospectrometer and transmission electron microscopy (TEM) images were captured on a JEOL JEM-100CX II machine operating at 100 kV ;

were grown from a concentrated dichloromethane solution after a few days storage at $-18\text{ }^{\circ}\text{C}$. $[\text{Bi}(\text{dbm})_3]_2$ crystallized in the triclinic space group $P\bar{1}$ as an oxygen-bridged centrosymmetric dimer (Fig. 2).

The inversion point lies at the heart of the Bi_2O_2 ring at the centre of the molecule. Each bismuth centre is formally 7-coordinate however, with the lone pair on bismuth, there are 8 valence pairs of electrons thus the coordination geometry of $[\text{Bi}(\text{dbm})_3]_2$ is based on an 8 valence pair compound. The arrangement of electron pairs best fits a square antiprism, with the degree of distortion away from an ideal square antiprism shown in Fig. 3.

Further details on the crystal structure of $[\text{Bi}(\text{dbm})_3]_2$, including commentary on bond distances and angles compared to other bismuth(III) β -diketonate complexes, are available in the Supplementary information.

3.2. Aerosol-assisted chemical vapour deposition

3.2.1. Bismuth oxide

Deposition of Bi_2S_3 [23] and Bi_2Se_3 [24] via AACVD have previously been reported but this technique has not been applied to synthesis of Bi_2O_3 . $[\text{Bi}(\text{thd})_3]_2$ has been used to deposit bismuth oxide films via liquid-injection CVD but only with oxygen as a co-reactant [12] and $[\text{Bi}(\text{fod})_3]_2$ has been used for CVD without a co-reactant, however only bismuth films were deposited in this case [21]. In contrast the use of $[\text{Bi}(\text{dbm})_3]_2$ as a single-source precursor (Thermogravimetric Analysis of $[\text{Bi}(\text{dbm})_3]_2$ is reported in Supplementary information) deposited yellow, crystalline bismuth oxide films via AACVD on glass and stainless steel substrates over a variety of substrate temperatures between 410 and $525\text{ }^{\circ}\text{C}$ (Table 1); no deposition was observed below $410\text{ }^{\circ}\text{C}$. Analytical results on both substrates were near identical and hence only the results for deposition on glass are presented below. All films displayed good coverage and were adherent, passing the Scotch tape test but being removed by abrasion with steel wool. No visual changes in the films were noticed after prolonged storage in air.

Film growth rates were ca. 75, 280, 530 and 610 nm h^{-1} at 410, 450, 495 and $525\text{ }^{\circ}\text{C}$ respectively and increased exponentially with increasing temperature with apparent activation energy of 82.7 kJ mol^{-1} . This is somewhat higher than the activation energy

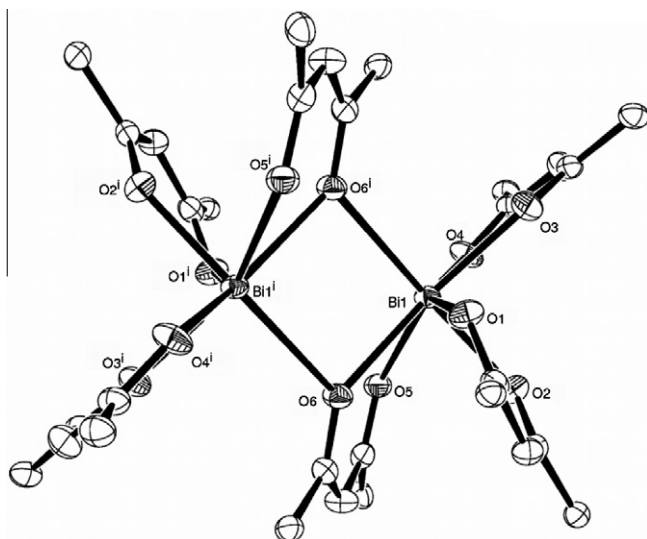


Fig. 2. ORTEP diagram showing the dimeric nature of $[\text{Bi}(\text{dbm})_3]_2$. Thermal ellipsoids at 50% probability, phenyl rings (bar ipso carbons), one CH_2Cl_2 solvent of crystallization and hydrogen atoms omitted for clarity. Atoms labelled 'i' are related by the symmetry code $1 - x, 1 - y, 1 - z$.

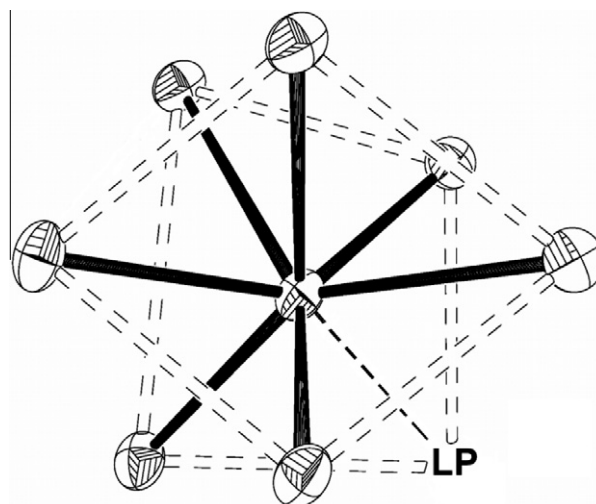


Fig. 3. Diagram representing the 8 valence pairs of electrons around bismuth in a distorted square antiprismatic geometry. LP = stereochemically active lone pair.

Table 1

AACVD film growth conditions for Bi_2O_3 thin films grown on glass substrates from $[\text{Bi}(\text{dbm})_3]_2$.

Substrate temperature ($^{\circ}\text{C}$)	Thickness (nm)	Crystalline phase	Band gap (eV)
410	75	β	2.4
450	280	β	2.4
495	530	β	2.3
525	610	β	2.5

measured for the deposition of α - Bi_2O_3 films on silicon substrates using $[\text{Bi}(\text{thd})_3]_2$ as a precursor (62.8 kJ mol^{-1}) using direct-liquid-injection CVD [12], however this is not unexpected due to differences in precursor concentration and mass transport in the two systems. Band-gaps were calculated (for films on glass only) from UV-Vis transmission spectroscopy using Tauc plots [27]. The band gap values fell in the visible range of the spectrum between 2.3 and 2.5 eV and are in good agreement with measured band-gap values obtained for β - Bi_2O_3 films obtained via LPCVD [4].

Film composition was measured using wavelength dispersive analysis of X-rays (WDX) however bismuth to oxygen ratios could not be determined due to breakthrough to the glass substrate and the presence of carbon contamination could not be ruled out as the insulating nature of the films required coating before analysis, preventing accurate determination of carbon content. The X-ray diffraction pattern of a Bi_2O_3 film deposited on glass at $450\text{ }^{\circ}\text{C}$ is shown in Fig. 4. All peaks can be matched to β - Bi_2O_3 , and the tetragonal unit cell parameters are in agreement with literature values [25] ($\alpha = \beta = 7.72(2)\text{ \AA}$, $\gamma = 5.62(2)\text{ \AA}$, JCPD Card No. 027-0050), with similar results found across the temperature range examined.

SEM (Fig. 5) of a Bi_2O_3 film deposited on glass at $450\text{ }^{\circ}\text{C}$ displays a globular morphology containing spherical bismuth oxide particles that are approximately 80 nm in diameter. This morphology is quite different to that observed for β - Bi_2O_3 films obtained via LPCVD which had non-uniform grains composed of triangular crystallites [4], although it is consistent with morphologies seen for AACVD deposited oxide thin films [26].

3.2.2. Platinum

We found the optimum temperature for deposition of platinum(0) films to be $410\text{ }^{\circ}\text{C}$. Platinum films were adherent to the

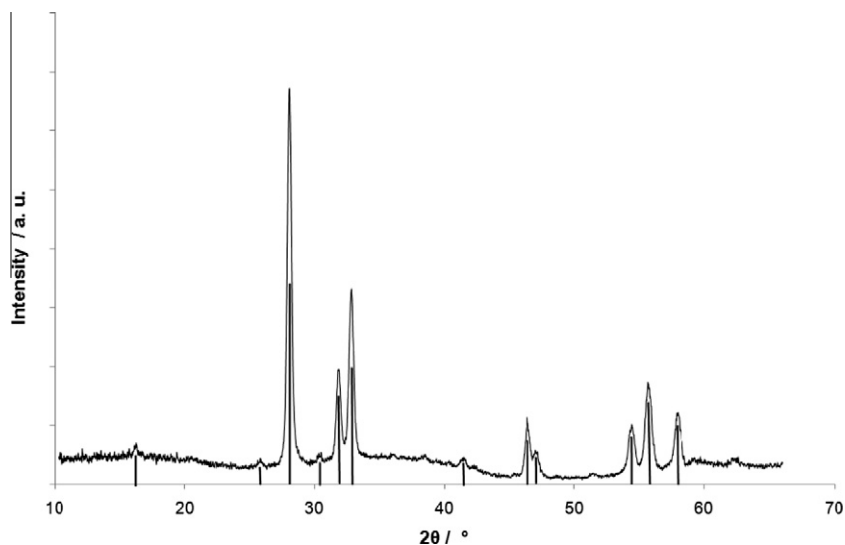


Fig. 4. XRD pattern of film deposited at 450 °C on a glass substrate; reflection planes for β - Bi_2O_3 (JCPD Card No. 027-0050) shown.

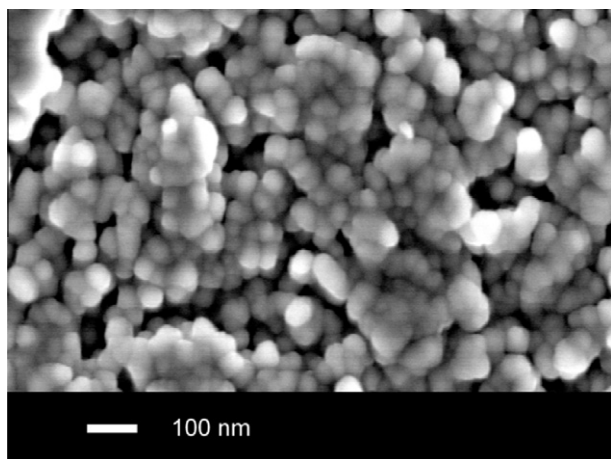


Fig. 5. SEM micrograph of a Bi_2O_3 film deposited at 450 °C on a glass substrate showing globular morphology.

substrate however they could be removed with mild abrasion. WDX analysis revealed chlorine contamination within the films to be negligible (less than 1 at.%). An XRD pattern of a platinum film deposited at 410 °C on glass is shown in Fig. 6 and consists of only two peaks, assigned to platinum metal (JCPD Card No. 004-0802); the low signal to noise ratio and high background between 20° and 30° 2θ is due to the glass substrate.

SEM imaging of a platinum film deposited at 410 °C (Fig. 7) reveals a morphology consisting of particles approximately 200–400 nm in diameter alongside smaller features roughly 100 nm diameter.

To prepare samples for TEM analysis depositions were performed on KBr substrates. XRD, SEM and WDX were consistent with results obtained during deposition on glass. The disc was dissolved in distilled water to remove KBr, leaving the platinum behind for imaging. The TEM image (Fig. 8) shows individual, well-defined platinum particles of approximately 4–10 nm in size whilst estimation of the particle size from XRD data (Scherrer equation) gave a value of ~ 10 nm. These results suggest the features observed in SEM (Fig. 7) are agglomerates of Pt nanoparticles.

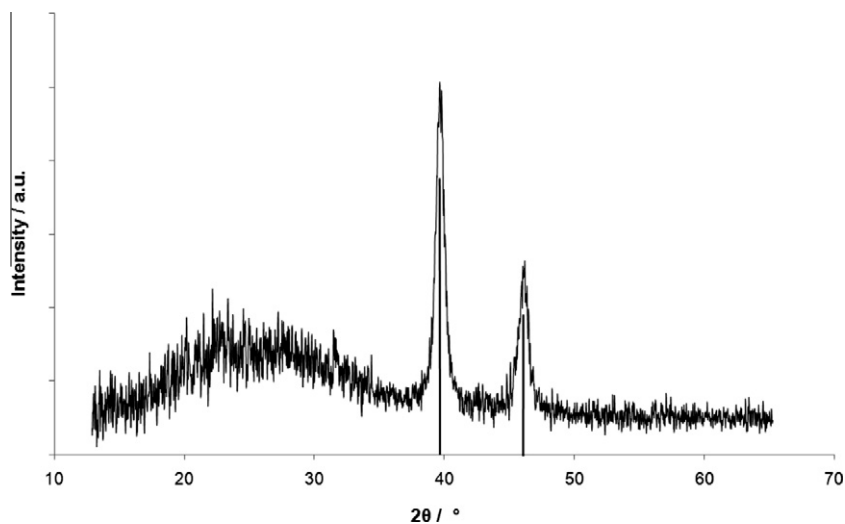


Fig. 6. XRD pattern of a film deposited at 410 °C on a glass substrate; reflection planes for Pt (JCPD Card No. 004-0802) highlighted.

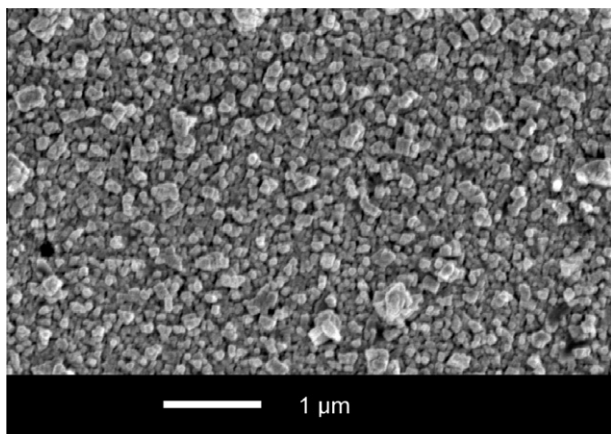


Fig. 7. SEM image of a platinum film deposited at 410 °C on a glass substrate.

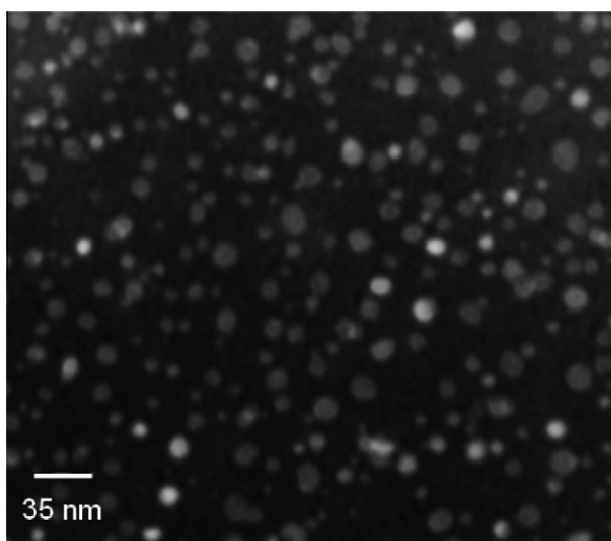


Fig. 8. TEM image of platinum nanoparticles deposited at 410 °C on a KBr substrate.

3.2.3. Co-deposited platinum and bismuth oxide

Pt–Bi₂O₃ films were obtained from co-deposition of [Bi(dbm)₃]₂ and H₂PtCl₆·6H₂O on steel substrates at 450 °C. WDX analysis showed the films were slightly oxygen deficient (stoichiometry Bi₂O_{2.8}) which is similar to β-Bi₂O₃ films found in the literature [4] and they contained an average of 0.36 at.% Pt in Bi₂O_{2.8} (0.89 at.% as a fraction of bismuth only). Chlorine contamination was negligible (<1 at.%) in these films, which is somewhat surprising given the heavy chlorine contamination observed when using glass as a substrate (Supplementary information), and as a result the concomitant formation of BiOCl was not observed for samples deposited on steel. The cause of this variability is not immediately obvious, particularly given that results for deposition of Bi₂O₃-only thin films were nearly identical irrespective of the substrate used.

X-ray diffraction (Fig. 9) of the films deposited on stainless steel revealed the presence of β-Bi₂O₃ as the dominant crystalline phase. Unit cell parameters were consistent with the values obtained for deposition of Bi₂O₃-only and are in agreement with literature values { $\alpha = \beta = 7.77(2)$ Å, $\gamma = 5.65(2)$ Å, JCPD Card No. 027-0050} [25]. The high, rising background observed in the pattern is due to fluorescence of the iron atoms present in the steel. Substrate peaks were clearly identified in the X-ray patterns, with no secondary phases of bismuth oxide and no peaks corresponding to platinum(0) observed. The lack of peaks for platinum is perhaps not

surprising given the relatively low amount of platinum present in these Pt–Bi₂O₃ samples (0.36 at.% based on Bi₂O_{2.8}).

SEM showed the films to be composed of globular particles similar to those obtained for Bi₂O₃-only samples (Fig. 5) and TEM (of samples deposited on KBr substrates) showed individual dispersed platinum nanoparticles, with average diameter of 5 nm or less, visible on the surface of much larger bismuth oxide crystallites. No equivalent features were observed in TEM of Bi₂O₃-only samples.

The composition of a Pt–Bi₂O₃ film deposited at 450 °C on stainless steel was studied using X-ray Photoelectron Spectroscopy. From the surface scan the bismuth 4f_{7/2} ionisation was at 158.9 eV and the O1s ionisation at 529.6 eV, both of which are characteristic of Bi₂O₃ [28]. The ratios of the areas of these peaks revealed slightly sub-stoichiometric Bi₂O_{2.7}, which is consistent with WDX analysis and is commonly found in β-Bi₂O₃ due to oxygen vacancies in the lattice [10]. Two distinct platinum peaks were observed at 71.5 (Pt 4f_{7/2}) and 74.8 (Pt 4f_{5/2}) eV which are characteristic of platinum(0) [29] and rule out formation of PtCl₂ or PtO_x [30]. This ionisation is not ascribed to Pt(OH)₂ as the Pt 4f_{7/2} ionisation would be expected at significantly higher energy (72.4 eV [30]) and the XRD of a Pt-only film deposited at 410 °C (Fig. 6) shows formation of platinum metal, hence we conclude the platinum is present in the Pt–Bi₂O₃ films as platinum metal. Carbon contamination was significant on the surface (~25 at.%) but decreased upon etching (~15 at.% after ~10 nm), however due to preferential sputtering quantification becomes unreliable and extensive etching was not performed.

AFM gave a value for root mean squared roughness (rms) of 97 nm. This is similar to reported values of indium–gallium oxide films formed via AACVD [26] but much higher than films of β-Bi₂O₃ (rms = 4.1 nm) deposited via low-pressure CVD [4]. The relatively high surface area obtained via AACVD is expected to be advantageous for catalytic purposes by giving a high contact area with the surrounding medium.

3.3. Water photolysis

Water photolysis was conducted using Bi₂O₃ and Pt–Bi₂O₃ samples deposited on stainless steel at 450 °C, with films of Pt deposited via AACVD and TiO₂ (anatase) deposited via atmospheric pressure CVD [31], both on stainless steel substrates, used to provide comparison (Table 2). Measurements were made in a sacrificial solution comprised of a 1:1 mixture of ethanol and water (results for a 1:1 mixture of ethanol and 0.1 M HCl are given in Supplementary information).

As expected non-platinised Bi₂O₃ samples produced no hydrogen upon illumination; it is apparent from Fig. 1 that the conduction band of Bi₂O₃ is too low in energy to reduce water to hydrogen at pH 0 and the use of a solution with near neutral pH is expected to exacerbate this problem. In fact this is the likely reason that no H₂ evolution is observed for the TiO₂ sample, despite the fact H₂ evolution was observed from the solution containing HCl (Supplementary information), with the evolution of H₂ becoming increasingly thermodynamically unfavourable with increasing pH. No hydrogen evolution was observed over Pt films however Pt–Bi₂O₃ thin films produced an average of 3.1 μmol H₂ h⁻¹ m⁻². This represents an apparent quantum efficiency of 0.6% (at 420 nm) and is of the order of those obtained using powdered catalysts CdS–ZnS and Pt–TaON:Pt–WO₃ [32]. Although the rate of H₂ evolution is low it should be highlighted these films have not been optimised in terms of film thickness or platinum loading. Previously it has been suggested that β-Bi₂O₃ is unstable to conversion to α-Bi₂O₃ under photo-irradiation [33] but we observed no visual degradation of any of the Bi₂O₃ or Pt–Bi₂O₃ samples during repeated irradiation in the ethanol:water solution and XRD analysis of films after photocatalytic testing showed the only phase present was

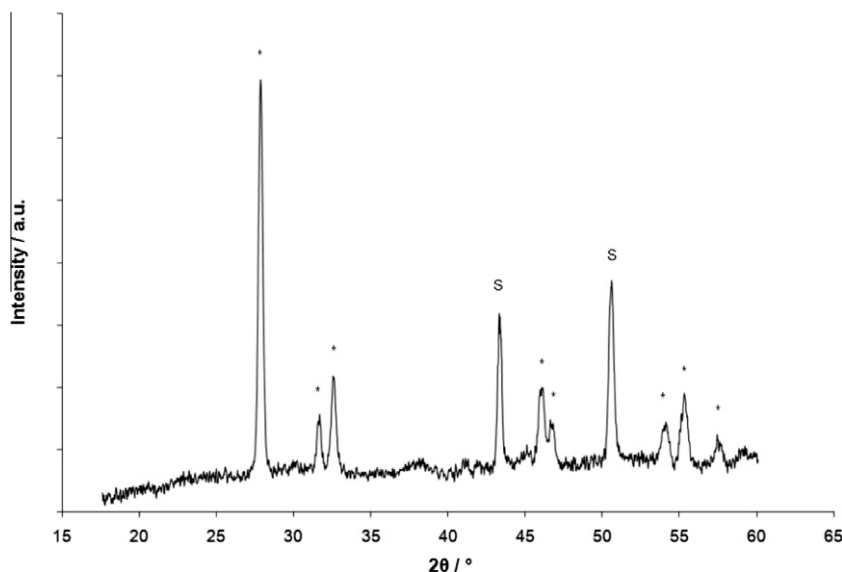


Fig. 9. X-ray diffraction pattern of Pt-Bi₂O₃ film deposited at 450 °C on a stainless steel substrate. Asterisks (*) refer to β-Bi₂O₃ peaks whereas peaks marked S correspond to the steel substrate.

Table 2

Rates of H₂ evolution on irradiation of samples immersed in 1:1 solution of ethanol and water.

Material	Rate of H ₂ production (μmol h ⁻¹ m ⁻²)
Pt	0
Bi ₂ O ₃	0
Pt-Bi ₂ O ₃	3.1
TiO ₂	0

β-Bi₂O₃, hence we conclude under these conditions β-Bi₂O₃ is photostable.

Neither thin films of platinum nanoparticles or of β-Bi₂O₃ evolved H₂ during water photolysis, therefore the ability of composite Pt-Bi₂O₃ to photo-reduce water is a property not contained by the constituent components. There is currently great interest in plasmon resonance enhancement of semiconductor photo-catalytic performance [34] and recently powdered Pt-Bi₂O₃ has been shown to be a highly active catalyst for photo-oxidation [35]. This has been ascribed to plasmonic enhancement of the photo-reaction, despite the fact that platinum nanoparticles have not previously been reported to have plasmonic properties. Plasmon enhancement causes increased light absorption, i.e. potentially increased quantum efficiency, but would not affect the thermodynamic potential of the Bi₂O₃ conduction band and therefore this effect alone would not be expected to enable photo-reduction of water over Pt-Bi₂O₃. We conclude the mechanism for the evolution of hydrogen must be *via* photon capture in the Bi₂O₃ followed by electron transfer to the Pt particles where they are trapped, this charge accumulates until the Pt particles become reducing [6].

4. Conclusions

We have synthesised a novel, moisture stable homoleptic bismuth(III) β-diketonate complex [Bi(dbm)₃]₂ which has been used as a single-source precursor to bismuth oxide films *via* AACVD. We have reported the use of H₂PtCl₆·6H₂O as a precursor to platinum nanoparticles *via* AACVD and we have demonstrated its use *via* co-deposition in conjunction with [Bi(dbm)₃]₂ to deposit thin films of platinum nanoparticle-doped bismuth oxide *via* AACVD. The Pt-Bi₂O₃ composite films photo-reduced water under

simulated solar irradiation, which is attributed to photon capture within the Bi₂O₃ followed by electron transfer to the Pt nanoparticles upon which the water reduction occurs.

Acknowledgements

The EPSRC and UCL are thanked for a Studentship (SM). The Leverhulme Trust is thanked for support *via* Research Project Grant F/07134/DB. Thanks go to Mr. K. Reeves for assistance with SEM measurements and to Dr. S. Firth for assistance with TGA experiments. Dr. Emily Smith (University of Nottingham) is thanked for carrying out XPS analysis under EPSRC Grant EP/F019750/1: "A Coordinated Open-Access Centre for Comprehensive Materials Analysis."

Appendix A. Supplementary material

CCDC 837634 contains the supplementary crystallographic data for this paper. These data can be obtained free of charge from The Cambridge Crystallographic Data Centre via www.ccdc.cam.ac.uk/data_request/cif. Supplementary data associated with this article can be found, in the online version, at [doi:10.1016/j.ica.2011.09.029](https://doi.org/10.1016/j.ica.2011.09.029).

References

- [1] A. Bard, M. Fox, *Acc. Chem. Res.* (1995) 141.
- [2] A. Walsh, G. Watson, D. Payne, R. Edgell, J. Guo, P.-A. Glans, T. Learmonth, K. Smith, *Phys. Rev. B* 73 (2006) 1.
- [3] L. Leontie, *Surf. Sci.* 507–510 (2002) 480.
- [4] S.J.A. Moniz, C.S. Blackman, C.J. Carmalt, G. Hyett, *J. Mater. Chem.* 20 (2010) 7881.
- [5] P.V. Kamat, *J. Phys. Chem. C* 111 (2007) 2834.
- [6] A. Mills, S.K. Lee, *Platin. Met. Rev.* 47 (2003) 2.
- [7] S. Vallejos, T. Stoycheva, P. Umek, C. Navio, R. Snyders, C. Bittencourt, E. Llobet, C. Blackman, S. Moniz, X. Correig, *Chem. Commun.* 47 (2011) 565.
- [8] A. Schweizer, G. Kerr, *Inorg. Chem.* 17 (1978) 2326.
- [9] P.A. Williams, A.C. Jones, M.J. Crosbie, P.J. Wright, J.F. Bickley, A. Steiner, H.O. Davies, T.J. Leedham, G.W. Critchlow, *Chem. Vap. Deposition* 7 (2001) 205.
- [10] G. Bandoli, D. Barreca, E. Brescacin, G.A. Rizzi, E. Tondello, *Chem. Vap. Deposition* 2 (1996) 238.
- [11] C. Bedoya, G.G. Condorelli, G. Anastasi, A. Baeri, F. Scerra, I.L. Fragalà, J.G. Lisoni, D. Wouters, *Chem. Mater.* 16 (2004) 3176.
- [12] S. Kang, *Thin Solid Films* 468 (2004) 79.
- [13] Bruker, SMART, SAINT and SADABS. Bruker AXS Inc., Madison, Wisconsin, USA, Version 2 (2006).

- [14] P. Van der Sluis, A.L. Spek, *Acta Crystallogr., Sect. A* 46 (1990) 194.
- [15] L.J. Farrugia, *J. Appl. Crystallogr.* 32 (1999) 83.
- [16] T. Hatanpää, M. Vehkamäki, M. Ritala, M. Leskelä, *Dalton Trans. (Cambridge, England: 2003)* 39 (2010) 3219.
- [17] G. Hyett, J.A. Darr, A. Mills, I.P. Parkin, *Chem. Vap. Deposition* 16 (2010) 301.
- [18] S. Elouali, A. Mills, I.P. Parkin, E. Bailey, P.F. McMillan, J.A. Darr, *J. Photochem. Photobiol., A* 216 (2010) 110.
- [19] M.-C. Massiani, R. Papiernik, L.G. Hubert-Pfalzgraf, J.-C. Daran, *Polyhedron* 10 (1991) 437.
- [20] L. Armelao, G. Bandoli, M. Casarin, G. Depaoli, E. Tondello, A. Vittadini, *Inorg. Chim. Acta* 276 (1997) 340.
- [21] K.C. Brooks, S.B. Turnipseed, R.M. Barkley, R.E. Sievers, J.V. Tulchinsky, A.E. Kaloyeros, *J. Chem. Mater.* (1992) 912.
- [22] A. Pisarevsky, in: *AIP Conference Proceedings*, 1992, p. 231.
- [23] J. Waters, D. Crouch, J. Raftery, P. O'Brien, *Chem. Mater.* 16 (2004) 3289.
- [24] A.A. Tahir, M.A. Ehsan, M. Mazhar, K.G.U. Wijayantha, M. Zeller, A.D. Hunter, *Chem. Mater.* 22 (2010) 5084.
- [25] H.A. Harwig, *Z. Anorg. Allg. Chem.* 444 (1978) 151.
- [26] C.E. Knapp, G. Hyett, I.P. Parkin, C.J. Carmalt, *Chem. Mater.* (2011) 1719.
- [27] J. Tauc, R. Grigorovici, A. Vancu, *Phys. Status Solidi B* 15 (1966) 627.
- [28] V.S. Dharmadhikari, S. Sainkar, S. Badrinarayan, A. Goswami, *J. Electron Spectrosc. Relat. Phenom.* 25 (1982) 181.
- [29] T. Morikawa, T. Ohwaki, K-ichi Suzuki, S. Moribe, S. Tero-Kubota, *Appl. Catal., B* 83 (2008) 56.
- [30] J. Hammond, N. Winograd, *J. Electroanal. Chem. Interf. Electrochem.* 78 (1977) 55.
- [31] G. Hyett, J.A. Darr, A. Mills, I.P. Parkin, *Chem. – A. Eur. J.* 16 (2010) 10546.
- [32] A. Kudo, Y. Miseki, *Chem. Soc. Rev.* 38 (2009) 253.
- [33] Y. Wang, Y. Wen, H. Ding, Y. Shan, *J. Mater. Sci.* 45 (2009) 1385.
- [34] Z. Liu, W. Hou, P. Pavaskar, M. Aykol, S.B. Cronin, *Nano Lett.* 11 (2011) 1111.
- [35] R. Li, W. Chen, H. Kobayashi, C. Ma, *Green Chem.* 12 (2010) 212.